Enhanced Diffusion at Intermediate Stereochemical Composition in Polypropylene by Dynamical Monte Carlo

Numan Waheed, Wayne L. Mattice,* and Ernst D. von Meerwall

Maurice Morton Institute of Polymer Science, The University of Akron, Akron, Ohio 44325-3909

Received October 3, 2006; Revised Manuscript Received December 18, 2006

ABSTRACT: We conduct a comprehensive study of the effect of stereochemistry on the diffusion of isotactic, atactic, and syndiotactic polypropylene (PP), with dynamical Monte Carlo. We simulate realistic two-bead Monte Carlo moves on a stereochemistry-dependent, coarse-grained model of PP based on the rotational isomeric state (RIS) model and repulsive Lennard-Jones interactions. We find that isotactic PP (iPP) diffuses faster than syndiotactic PP (sPP) as expected, but a maximum in the diffusion rate at an intermediate stereochemical composition (aPP) is also found. To determine the origin of this effect, we compare pair correlation functions of the slowest-moving beads to those of all beads, identifying conformations that limit mobility. We find a few small, long-lived clusters with chain conformations reminiscent of those in crystals in iPP and sPP; although slow-moving beads also cluster in aPP, they are short-lived with no dominant conformations. We look at the effects of local stereochemistry through Monte Carlo acceptance rates, categorized by the stereochemistry of the local tetrad and overall stereochemical composition. Sequences of *meso* and *racemo* diads diffuse faster in aPP due to quenched randomness of stereochemical sequences than in iPP and sPP. Comparison to isolated chain acceptance rates suggests that intermolecular cohesiveness of stereochemically pure sequences lowers mobility but can be overcome by the randomness of atactic stereochemistry. The mechanisms described here for PP may affect the mobility of other polymers in which stereochemical composition is an issue.

Introduction

The stereochemistry of polymer chains is fundamental to understanding their dynamic properties, but surprisingly little has been quantified regarding stereochemical composition within the spectrum of "atactic" vinyl polymers. For the prototypical case of polypropylene (PP), it is well-known that isotactic (iPP) and syndiotactic (sPP) chains yield different equilibrium properties, including the relaxation time, the entanglement molecular weight, and the glass transition temperature, but atactic chains are often characterized as similar in melt behavior to isotactic chains, without delving into the significance of random stereochemistry.[1,2] Although stereochemical effects are well understood for mixtures of small-molecule enantiomers, the bonding of enantiomers together into atactic chains adds the complexity of quenched randomness within the chain, which has been studied in the context of the dimensions of vinyl polymers[3] as well as in other polymer contexts.[4,5] Atactic chains, although consisting of chemically identical monomers, are actually random copolymers, as pointed out by Flory.[6] Even monodisperse atactic chains usually have differing fractions of *meso* and *racemo* diads, indicating that each one has a unique conformational partition function describing it. Because of the complexity in detailing with stereochemistry experimentally, chains consisting of an intermediate mixture of diads are labeled simply as "atactic",[2,7,8] such that comparison of samples becomes difficult. Therefore, there is a need for a more comprehensive study of the effects of dynamics as a function of the probability of a *meso* diad P_m, covering the range of pure and intermediate stereochemical compositions.

Molecular simulation has an advantage when studying the effects of stereochemical composition on diffusion in PP because it gives us the capability to control stereochemistry precisely. The local dynamics of iPP and sPP have previously been studied using molecular dynamics.[9,10] In addition, simulation methodologies have evolved, such that we can now use coarse-grained models of polypropylene, based on the rotational isomeric state (RIS) model, that maintain stereochemical specificity.[11] Several equilibrium studies of miscibility and tacticity using polypropylene have been recently conducted using this method.[12−16] More recently, we have refined our Monte Carlo methods to sample realistic dynamics by constructing physical moves that preserve the mapping to real time.[17] This dynamical Monte Carlo technique allows for the efficient study of the relationship between melt diffusion and stereochemical composition.

In this work, we conduct dynamical Monte Carlo simulations of melt density polypropylene at variable stereochemical compositions. We compute relative diffusion rates as a function of the probability of a *meso* diad. We examine the distribution of displacements of atoms over time in order to determine the origin of the stereochemical effects, as well as the length correlations between unmoved beads, to identify clustering of slow-moving conformations. In addition, we study the acceptance rates of moves based on the local stereochemical sequence at the bead. By comparing acceptance rates of melt density chains to those of isolated chains, the importance of the stereochemically governed intramolecular conformation vs intermolecular packing effects is assessed.

Computational Method

Chain Representation. Polypropylene chains are modeled by a surrogate chain of 25 bonded beads, each bead representing a C_3H_6 monomer unit. All chains are deliberately shorter than the entanglement length for PP to isolate stereochemical effects.[1] These coarse-grained beads are centered on the backbone carbon atom that is bonded to the methyl side group. Because the carbon atoms exhibit tetrahedral geometry, the coarse-grained beads, which represent two backbone carbons, can be placed on the high-coordination second-nearest-neighbor diamond (2NND) lattice, which is constructed by removing alternating sites from

* To whom correspondence should be addressed: e-mail wlm@polymer.uakron.edu; Tel (330) 972-5128; Fax (330) 972-5396.

10.1021/ma062285r CCC: $37.00
Published on Web 02/02/2007

Table 1. Summary of Systems Simulated (T = 453 K in All Cases)

P_m[a]	replicas[b]	density (g/cm^3)	N_{chain}[c]	N_{bead}[d]	LJ shells[e]
0.0,0.2,0.4,0.6,0.8,1.0	3	0.73 (melt)	64	25	2
0.0,0.2,0.4,0.6,0.8,1.0	3	0.73 (melt)	64	25	3
0.0,0.2,0.4,0.6,0.8,1.0	3	0.00086 (isolated chain)	1	100	2

[a] Simulations were performed for each of the stereochemical compositions listed. [b] Number of independent simulations at each P_m. [c] Number of independent parent chains. [d] Number of beads per chain. [e] Two shells incorporate only the repulsive core of the LJ potential. The region including the minimum in the potential is included when the LJ potential is represented by three shells.

the tetrahedral diamond lattice.[18] A melt density of 0.73 g/cm^3 is achieved by simulating 64 PP chains on a 24 × 24 × 24 unit cell, with a lattice spacing of 2.5 Å, to best match the experimental melt density of 0.75 g/cm^3 for PP in this temperature range.[19] Temperature is regulated to 453 K through the choice of density and the determination of statistical weights and the LJ modification as follows, such that the ensemble is maintained under NVT conditions.

Intramolecular energies are modeled based on the three-state RIS model for PP developed by Suter et al.[20] The short-range statistical weights of conformations are determined by the RIS intramolecular energy and temperature through the Boltzmann factor. The first-order interactions are $E_\eta = 0.29$ kJ/mol and $E_\tau = 3.8$ kJ/mol, while the second-order effects are given by $E_\omega = 8.0$ kJ/mol, for the η, τ, and ω interactions as defined by Mattice and Suter.[21] By reverse-mapping from the 2NND lattice to the underlying tetrahedral lattice,[22] we rule out conformations that lead to the collapse of the PP chain on the underlying lattice.[11] The stereochemistry at the asymmetric stereochemical center is accounted for solely through the RIS probabilities since each coarse-grained bead is in a stereochemical configuration that dictates the dominant conformations, as described by Mattice and Suter.[21] The probabilities of the conformations at that site reflect the stereochemical configuration of the site and its two bonded neighbors.

Long-range intermolecular energies are given by a discretized Lennard-Jones potential,[23] parametrized for PP monomer units,[24] which quantifies the average Lennard-Jones energy for neighboring beads in each interaction shell ($10i^2 + 2$ neighbors for shell i). The shell energies are 26.851 kJ/mol for the first shell, 3.068 kJ/mol for the second shell, and −1.089 kJ/mol for the third shell. Because these were originally computed for a slightly higher temperature, this may represent a slightly higher repulsive energy than should be present at 453 K. For PP at melt density, only repulsive shells, the first and second, are used in order to speed up computation. This approximation is often appropriate for NVT simulations of melt density systems, where small interatomic distances are prevalent; some results from simulations with the attractive third shell are also included for comparison.

Single-chain simulations are also conducted to isolate intramolecular effects. Energies are governed by the same short-range RIS probabilities, modified by the long-range discretized Lennard-Jones. Three independent simulations of a single chain of monomer beads are modeled on a 100 × 100 × 100 unit lattice at each P_m. The longer chain is used to improve chain statistics, while the larger lattice is used to guarantee the isolation of the chain. The change in chain length is not an issue since we are only interested in the acceptance rates as a function of local stereochemistry for isolated chain simulations, of which chain length is a minimal factor. Intermolecular effects due to chain packing can be deduced by comparison of acceptance rates from the melt simulations to acceptance rates from the isolated chain simulations. The systems simulated are summarized in Table 1.

Dynamical Monte Carlo. Equilibration of the initial melt simulation is achieved through a Boltzmann-weighted chain building algorithm, followed by equilibrium Monte Carlo simulation that rapidly samples phase space, both described below. Bead stereochemical configurations are chosen randomly according to the probability of *meso* diad for the system, assuming Bernoullian statistics, for each of the six stereochemical compositions explored. The occupancy of the lattice is low, near 12% at melt density, which allows systems to be built by random placement of the initial bead of a chain, followed by placement of subsequent beads weighted by the stereochemistry-dependent RIS probabilities of each possibility. Chain overlaps are prohibited. Further equilibration of the long-range energy is achieved by Monte Carlo simulation, using single bead moves[22] and 2−6 bead pivot moves[24] for 5 million Monte Carlo steps. These moves provide an efficient sampling of phase space to reach an equilibrated system. The larger pivot moves, however, allow chain crossing during moves, which make the moves aphysical and unsuitable for simulation of dynamics.

The simulation of dynamics exclusively utilizes two-bead rotation moves, designed to mimic physical moves and prevent chain crossing, leading to accurate dynamic rate data.[17] The two-bead moves not only improve computational time over single bead moves but also realistically model the coupled movement of bonded beads. Single bead moves are included implicitly in the two-bead moves since all possible locations of the two bonded beads are considered. The details of implementing the two-bead moves on the 2NND lattice are discussed elsewhere.[17] Four million Monte Carlo steps of dynamics are conducted for the melt simulations. For the isolated chain simulations, equilibration is almost complete through the chain building algorithm; therefore, only the 4 million Monte Carlo steps of dynamics are conducted.

One Monte Carlo step consists of the average number of moves required to attempt to move every bead once, although the actual beads that are moved are chosen at random. (For equilibration, one Monte Carlo step attempts to move every bead once by single bead moves as well as once by pivot moves.) The probability of a configuration is computed from RIS statistical weights, modified by the additional long-range energy of neighbor interactions. An alternative configuration is randomly chosen out of all possible alternatives. Then move acceptance is determined by comparison of the probabilities of initial and final states through the Metropolis criterion. Applying this criterion to dynamical Monte Carlo assumes that the differences in the activation energy barrier for all moves are insignificant.

While the dynamical Monte Carlo algorithm is suited for representation of dynamics since the steps are proportional to real time, the proportionality factor is not known a priori. Therefore, we will present results in units of Monte Carlo steps (MCS). Diffusion information is presented relative to the diffusion coefficient found for iPP.

Analysis Methods. Relative diffusion coefficients for the melt are calculated from the mean-square displacements of center

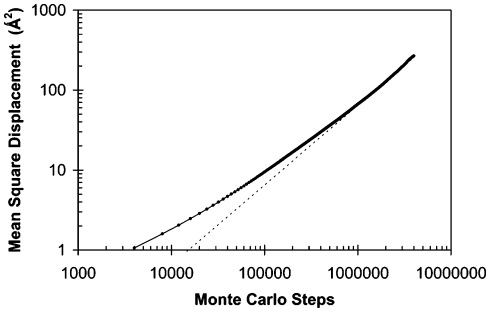

Figure 1. Averaged mean-square displacements of the centers of mass of chains with $P_m = 0.8$, as obtained from three independent simulations of a system at 453 K, each with 64 chains in the melt. Dotted line shows Fickian diffusion limit where the slope equals one.

of mass of each chain over time, based on the coordinates sampled at every 4000 MCS. Displacements over short times are sub-Fickian in nature, while fewer data points over long times result in poor statistics. Therefore, the data for mean-square displacements from 1.0 to 2.0 million MCS are used to compute the diffusion coefficient. The diffusion coefficient, defined rigorously as the infinite time limit of the derivative of the mean-square displacement with respect to time, is evaluated in the simulation using the center-of-mass coordinate of a chain, $\mathbf{r}_{com}$, at $t_0 = 1.0 \times 10^6$ MCS and $t_1 = 2.0 \times 10^6$ MCS.

$$D = \frac{1}{6}\lim_{t\to\infty}\frac{\mathrm{d}\langle \mathbf{r}_{com}(t)\cdot\mathbf{r}_{com}(t)\rangle}{\mathrm{d}t} \approx \frac{\langle[\mathbf{r}_{com}(t_1) - \mathbf{r}_{com}(t_0)]\cdot[\mathbf{r}_{com}(t_1) - \mathbf{r}_{com}(t_0)]\rangle}{6(t_1 - t_0)} \quad (1)$$

Three independent simulations at each of the six stereochemical compositions are conducted; each simulation provides 64 estimates for the diffusion coefficient, one from each chain. From the mean and variance of the measurements, the average diffusion coefficient and 90% confidence intervals are computed. Figure 1 depicts mean-square displacements of the centers of mass of the chains, averaged over 192 chains from the three independent replicas at $P_m = 0.8$, each with 64 chains in the melt.

In addition, data from select simulations are analyzed further to determine the distribution of square displacements of individual beads and the length correlations between slow-moving beads. The square displacements of individual beads take on discrete values based on the geometry of the lattice. The total number of observations at each of the discrete distances are tabulated and used to compute histograms at specific time intervals to determine the distribution of bead displacements over a certain time. We do not search only for beads that diffuse abnormally slowly at the beginning of the simulation, but instead search also for beads that diffuse slowly during any time period within the simulation. All beads can diffuse slowly at certain times, when they and their neighbors take on certain conformations randomly. When these conformations eventually change, they may return to the populations of faster diffusing beads.

To determine the origin of the slow-moving beads, the intermolecular pair correlation functions between unmoved beads over a time interval are also computed, by comparison to the ideal gas spherical shell volume expansion, based on the formula given in Allen and Tildesley:[25]

$$g(r) = \frac{V}{N}\frac{1}{4\pi r^2\,\mathrm{d}r}\left(\sum_i\sum_{j\neq i}\delta(r - r_{ij})\right) \quad (2)$$

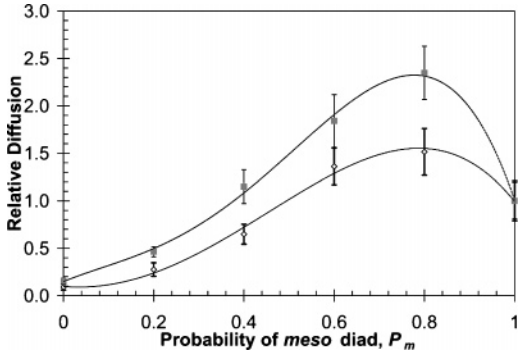

Figure 2. Relative diffusion coefficients as a function of the probability of *meso* diad for simulations without attractive shell (■) and with attractive shell (◇). $P_m = 0$ is sPP while $P_m = 1$ is iPP. Error bars are 90% confidence intervals. Values are normalized by the diffusion coefficient of iPP.

where V is the volume of the system, N is the number of beads in the system, and dr is the thickness of the volume shell being sampled. The discrete lattice distances are rendered as a Bezier curve of the nth degree, where n is the number of discrete lattice distances. These length correlations for unmoved beads are compared to the length correlations of the total system to determine whether the unmoved beads are clustering or evenly distributed. For intramolecular length correlations, the distribution of discrete lattice distances between beads that do not move are computed and compared to the distribution of distances between all beads. The discrete distances are then uniquely reverse-mapped to the torsional conformations of the underlying chains to determine which conformations are slow-moving for given stereochemical compositions.

Diffusion as a function of stereochemical composition can also be analyzed through the acceptance rates of Monte Carlo moves based on the local stereochemical configuration. Because the dynamic simulations use two-bead moves, the local stereochemistries are based on the stereochemical configurations at the two relocated bonded beads and their two bonded neighbors. This relationship is captured by three diads at the move site or the local tetrad. Only internal chain beads are considered. Therefore, we tabulate acceptance rates of internal chain moves based on the local tetrad: *mmm*, *mmr*, *rmr*, *mrm*, *rrm*, or *rrr*. Data are tabulated from 100 000 MCS from each of two independent initial stereochemistries (for intermediate stereochemical compositions). The acceptance rates are used as a measure of local chain mobility. The significance of inter- or intramolecular interactions is assessed by comparison of melt acceptance rates to acceptance rates of isolated chains from two independent simulations of 100 000 MCS each.

Results

Relative diffusion coefficients and 90% confidence intervals are obtained from the three independent simulations at each stereochemical composition, shown in Figure 2. Melt iPP ($P_m = 1$) diffuses faster that melt sPP ($P_m = 0$), which is a well-understood difference due to the dominant conformations for each stereochemistry.[2,7,8] However, at intermediate stereochemical composition an unexpected maximum is observed near $P_m = 0.75$. To verify that this effect is not due to the repulsive-only simulations, additional runs were conducted including the attractive third shell and are included in Figure 2 as well. The values are shown normalized to the diffusion of iPP. When comparing the simulations with and without the third shell, it is worth noting that the absolute values of the diffusion coefficient are ~7 times higher without the repulsive shell as they

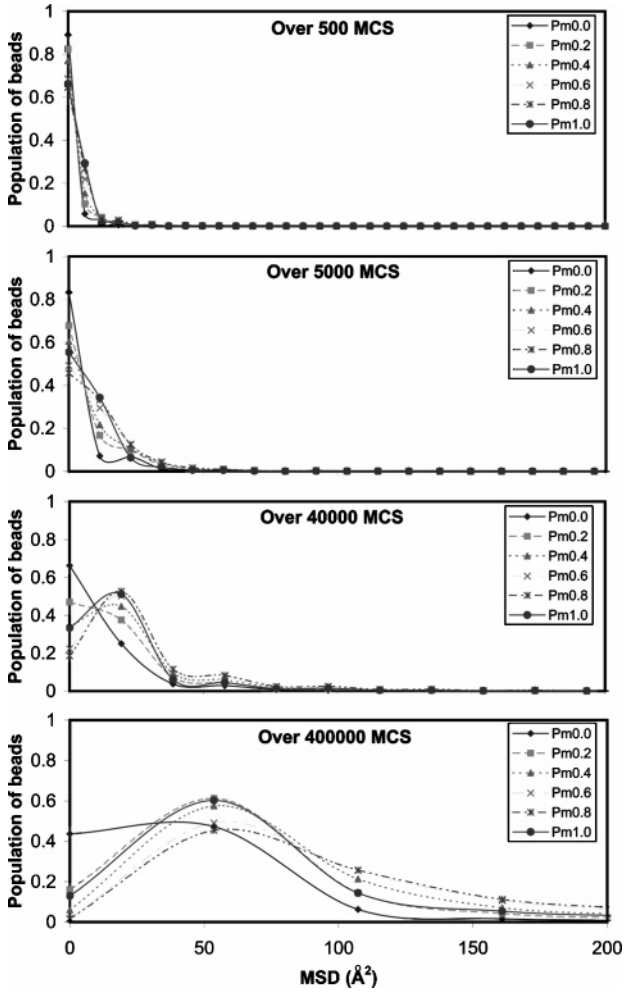

Figure 3. Distribution of square displacements of individual atoms over the intervals of 500 MCS (top panel), 5000 MCS (second panel), 40 000 MCS (third panel), and 400 000 MCS (bottom panel), for six values of the probability of *meso* diad P_m.

are with the repulsive shell. The attractive part of the LJ potential produces a stickiness to the interchain interaction that provides cohesion, thereby changing the relationship between MCS and real time. It is also responsible for the mixing behavior of PP melts.[14] On the basis of a prior quantitative comparison of mixing behavior of PP melts in experiment and simulation,[14] the true value of the energy for the third shell is likely to lie between the two limits used in Figure 2; i.e., it is between 0 and −1.089 kJ/mol. The time constants for the decay of autocorrelation function of the end-to-end vector (not shown) were also found to have a P_m dependence consistent with the diffusion coefficients; the dependence of the time constant on P_m was inversely related to the dependence of the diffusion constant on P_m.

In addition, the distribution of square displacements of individual atoms over time, shown in Figure 3, reveals that the transition that occurs at short times, from a delta function at 0 MCS to a distribution of increasing displacements, has the hallmarks of a Poisson distribution over increasing time intervals. Over 500 MCS intervals, the majority of beads in the systems have not yet moved from their positions. The transition is evident in the second and third panel, as the number of unmoved beads decays and a unimodal distribution emerges, which is almost complete for all stereochemical compositions in the last panel, over 400 000 MCS intervals. The systems with an average probability of *meso* diad of 0.6 and 0.8 are the fastest to achieve this distribution, while the sPP ($P_m = 0$) system is

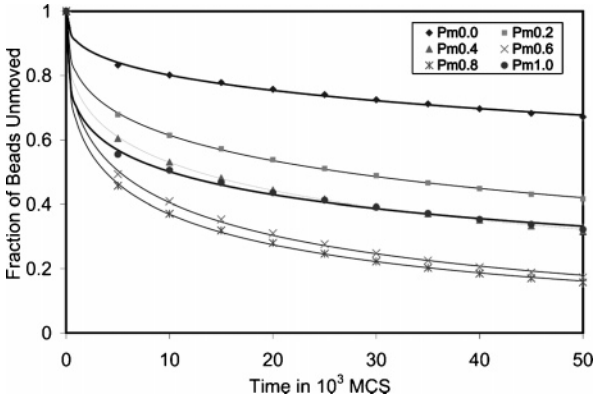

Figure 4. Decay of the function of unmoved beads over a time interval, for six values of the probability of *meso* diad P_m. Lines represent the fit to the KWW equation (eq 3) using the fitted parameter in Table 2.

Table 2. Fitted Parameters for the KWW Equation (Eq 3) for the Decay of the Fraction of Unmoved Beads over a Time Interval, for Six Simulations at Different Probability of *Meso* Diad

probability of *meso* diad	τ_{KWW} (10^5 MCS)	β
0.0	72.26	0.35
0.2	7.43	0.36
0.4	3.53	0.36
0.6	1.29	0.40
0.8	1.01	0.37
1.0	3.57	0.29

the slowest. However, the end distribution appears to be unimodal in all cases, and the distribution of square displacements is a Poisson distribution, regardless of stereochemistry, indicating that systems with pure stereochemistry do not behave fundamentally differently than the intermediate, random stereochemistry. This result does not suggest the reason for a maximum in the diffusion rate to be observed at intermediate stereochemical composition.

To determine the origin of the maximum, we turn our focus to the nature of the population of unmoved beads. We can calculate the decay of this population of unmoved beads over different time intervals in order to extract a time constant for the decay. Figure 4 shows the fraction of unmoved beads over time for each stereochemical composition. The initial rate of decay from all beads unmoved at $t = 0$ seems to be related to the overall diffusion rate. This decay is a stretched exponential that can be fitted by the Kohlrausch−Williams−Watts (KWW) equation:[26]

$$f_{KWW}(t) = \exp[-(t/\tau_{KWW})^{\beta}] \qquad (3)$$

The time constant τ_{KWW} and stretching factor β for this initial decay are shown in Table 2. The same trend was seen in the time constant for decay of the chain end-to-end vector autocorrelation function (not shown). Values in Table 2 reinforce the maximum in the diffusion rate as a function of stereochemistry, but the only new information is that unmoved beads persist longer through the simulation as the probability of *meso* diad approaches the two pure stereochemistries. Further spatial characteristics of the slow-moving beads are required for us to identify which conformations are responsible for the differences in decay rate due to stereochemical composition.

We identify the intra- and intermolecular length correlations between unmoved beads. However, in order to identify the slow-moving conformations, we need to select a time interval that yields a narrow subset of beads, but not so narrow that good statistics cannot be achieved. For each stereochemical composition, this time interval will be different since diffusion rates

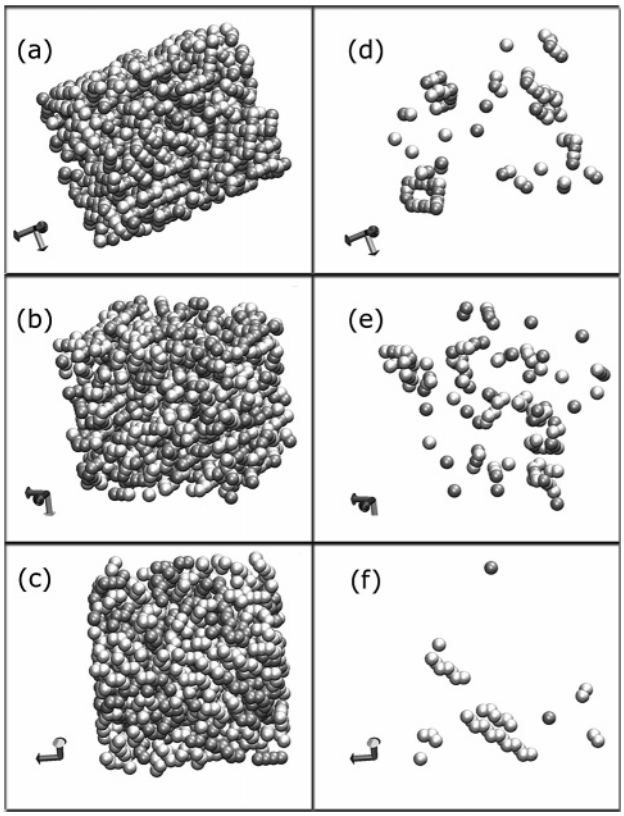

Figure 5. Instantaneous snapshots of iPP (a), aPP (b), and sPP (c) and the corresponding snapshots of unmoved beads over the time interval of 4.0×10^5 MCS for iPP (d), 8.0×10^4 MCS for aPP (e), and 3.2×10^6 MCS for sPP (f). Dark gray beads represent an *l*-configuration stereochemistry, and light gray are *d*-configurations (images rendered using Visual Molecular Dynamics,[27] version 1.8.3).

Table 3. Time Intervals in Monte Carlo Steps Required To Allow for Approximately 1−2% of Beads To Remain Unmoved and the Actual Percent of Unmoved Beads in These Intervals, for Three Simulations of Differing Stereochemical Composition

probability of *meso* diad	time interval (10^6 MCS)	% of beads unmoved
0.0	3.2	1.23
0.6	0.080	2.09
1.0	0.40	1.88

are different in each case. We try to identify time intervals during which 1−2% of total beads do not move (aiming for the slowest 20−30 beads) for three samples: iPP, sPP, and $P_m = 0.6$ as a representative for intermediate stereochemistry. Table 3 shows the time intervals we selected for each system and the average percent of unmoved beads during those time intervals. Figure 5 shows instantaneous snapshots of the iPP, sPP, and aPP systems as well as the corresponding snapshots of the beads that are unmoved in each system during the subsequent time interval appropriate for that system. If the selected beads are uniformly distributed, the distances between them would be 4−5 times larger than the value of σ in the LJ potential for propylene. Thus, the slowest-moving 1−2% of the beads will not cluster unless their movements are correlated.

Focusing on the intermolecular correlations between unmoved beads, the pair distribution functions $g(r)$, shown in Figure 6, between all pairs of unmoved beads for each stereochemical composition are compared to the pair distribution function for all beads. The function $g(r)$ is normalized by the average density of unmoved beads in each case (and for the total average density when looking at all beads). In all three cases, unmoved beads are more correlated at short lengths, between approximately 6

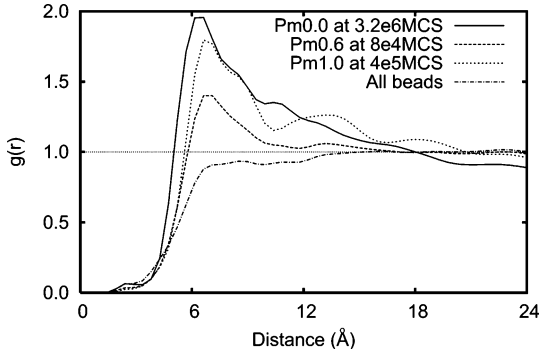

Figure 6. Intermolecular pair distribution function $g(r)$ for all pairs of beads in aPP (representative of correlations between all beads in sPP and iPP as well) (dotted-dashed line) and for pairs of unmoved beads over the interval of 4.0×10^5 MCS for iPP (dotted line), 8.0×10^4 MCS for aPP (dashed line), and 3.2×10^6 MCS for sPP (solid line).

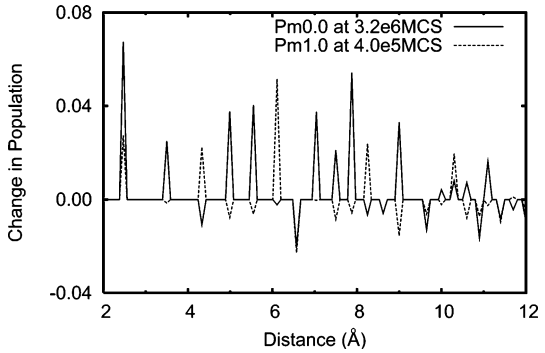

Figure 7. Difference in the fractional population of intramolecular distances between unmoved beads and the fractional population of intramolecular distances between all beads, over an interval of 4.0×10^5 MCS for iPP (dashed line) and 3.2×10^6 MCS for sPP (solid line).

and 18 Å, than all beads of the system are, suggesting that slow-moving beads are not well dispersed spatially, but instead cluster at shorter distances in all cases, showing signs of spatial heterogeneity. The correlations between all beads have a flattened $g(r)$ due to the repulsive-only potential; this reminder of the absence of an attractive potential makes the clusters of unmoved beads more surprising. In light of the time intervals presented in Table 3, we can say that the clusters of slow-moving beads for $P_m = 0.6$ are short-lived, compared to the clusters in the pure stereochemistries, and that the clusters in sPP are the longest-lived.

The intramolecular pair correlations reveal which conformations are clustering together. We calculate the fractional population of intramolecular distances between unmoved beads for iPP and sPP as well as the fractional population of intramolecular distances for all beads in these systems. Figure 7 shows the differences in the fractional populations of intramolecular distances between unmoved beads and all beads, for iPP and sPP, revealing certain distances that are more common among unmoved beads and certain distances that are less common for each stereochemistry. Because distances on the 2NND lattice can be mapped back to the tetrahedral lattice, we know the relationship between the intramolecular distances and the torsional conformations they represent, shown in Table 4. For the iPP case, the distances between unmoved beads that yield higher than normal populations, at 4.33, 6.12, and 8.29 Å, are sequences in the $tg^{\pm}$ helix, the most probable conformation for iPP. The most probable conformation of sPP is the zigzag planar conformation, consisting of *trans* states, but looking at Table 4 and Figure 7, sequences of *trans* states (which

Table 4. Relationship between Intramolecular Bead Distances on the 2NND Lattice and the Underlying Chain Conformations

Distances(A)[a]	2.50	3.54	4.33	5.00	5.59	6.12	6.61	7.07	7.50	7.90	8.29	8.65	9.01	9.99
1-2 conformations	$g^{\pm}g^{\mp}$	$g^{\pm}g^{\pm}$	$\boldsymbol{g^{\pm}t}$	$\boldsymbol{tt}$										
1-3 conformations	$g^{\pm}g^{\pm}g^{\mp}g^{\mp}$ $g^{\pm}g^{\pm}g^{\mp}g^{\pm}$ $g^{\pm}g^{\mp}g^{\mp}g^{\pm}$ $g^{\pm}g^{\mp}g^{\pm}t$	$g^{\pm}g^{\mp}g^{\mp}t$	$g^{\pm}g^{\pm}g^{\mp}g^{\mp}$ $g^{\pm}g^{\pm}g^{\mp}t$ $g^{\pm}g^{\pm}tg^{\pm}$ $g^{\pm}g^{\mp}tg^{\mp}$ $g^{\pm}g^{\mp}tt$	$g^{\pm}g^{\mp}tg^{\pm}$ $g^{\pm}ttg^{\mp}$ $tg^{\pm}g^{\mp}t$	$g^{\pm}g^{\pm}g^{\pm}g^{\pm}g$ $g^{\pm}g^{\pm}g^{\pm}t$ $g^{\pm}g^{\pm}tg^{\mp}$ $g^{\pm}g^{\pm}tt$ $g^{\pm}ttg^{\pm}$ $tg^{\pm}g^{\pm}t$	$\boldsymbol{g^{\pm}tg^{\pm}t}$	$g^{\pm}tg^{\mp}t$ $g^{\pm}ttt$ $tg^{\pm}tt$		$\boldsymbol{tttt}$					
1-4 conformations (dominant ones only)								$g^{\pm}g^{\pm}g^{\pm}g^{\pm}g^{\pm}g^{\pm}$ $g^{\pm}g^{\pm}ttg^{\pm}g^{\pm}$		$g^{\pm}g^{\pm}g^{\pm}g^{\pm}tt$	$\boldsymbol{g^{\pm}tg^{\pm}tg^{\pm}t}$	$g^{\pm}tg^{\mp}tg^{\pm}t$	$g^{\pm}ttttt$	$\boldsymbol{ttttt}$

[a] These distances can be generated by the given sequence of torsional states or its reverse sequence.

take the distances of 5.0, 7.5, and 10.0 Å on the 2NND lattice) cannot explain all the increased distances for sPP. In fact, the increased peaks reveal the prevalence of another probable conformation for sPP, $g^{\pm}g^{\pm}$, and distances between unmoved beads that have increased populations in Figure 7 are all combinations of *tt* and $g^{\pm}g^{\pm}$ sequences. For the atactic case of $P_m = 0.6$, which is not shown, the distances between unmoved beads shows increased populations of some peaks related to iPP and some related to sPP.

We complement our analysis of displacements with data on melt acceptance rates as a function of local tetrads. Sequences of *mmm* and *rrr* are the only sequences seen in iPP and sPP, respectively, but they also show up at intermediate stereochemistries due to the quenched randomness of stereochemical sequences. Surprisingly, moves involving *mmm* tetrads have a lower acceptance rate at pure stereochemistry ($P_m = 1.0$) compared to $P_m = 0.8$. This suggests that although iPP is more mobile than sPP, mobility is actually increased by random placement of *racemo* diads in iPP chains. A similar, but smaller, decrease in mobility is seen in sequences of *rrr* close to $P_m = 0$. Magnitudes for the melt acceptance rates of iPP ($P_m = 1.0$) are ~5 times greater than that for sPP ($P_m = 0.0$). For the intermediates *mmr*, *rmr*, *mrm*, and *rrm*, the dependence of the acceptance rates on the tetrad or fraction of *meso* diads in the tetrad is statistically difficult to discern.

Because the clusters of slow-moving beads have both intra- and intermolecular influences in all cases, we compare the acceptance rates of our melt systems to acceptance rates for isolated chains to determine how these effects lead to the maximum in diffusion and acceptance rates as a function of P_m in melt systems. Acceptance of moves in isolated chains is primarily a factor of the intramolecular RIS statistical weights; therefore, if the intramolecular effects cause the maximum, we will see a similar maximum in acceptance rates for isolated chains as well. The ratio between the melt acceptance rate and the isolated chain acceptance rate, therefore, yields a measure of the relation of the intramolecular contribution to the total effect. This ratio of melt acceptance rates to isolate acceptance rates is shown in Figure 8 for moves at each of the local tetrads. At intermediate stereochemical composition ($P_m = 0.2-0.8$), this ratio takes on values that are almost statistically equivalent, except for the ratio for *rrr* tetrads at $P_m = 0.2$; the average 90% confidence interval across the entire intermediate stereochemical composition range is given as the error bar for the overall average ratio of 0.74 in this range and is shown near $P_m = 0.85$ in Figure 8. For all the tetrads, when they are in the

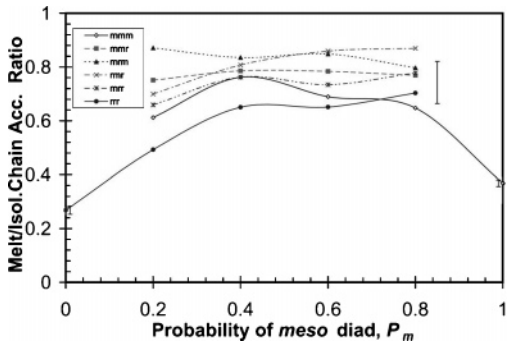

Figure 8. Ratio of melt acceptance rates to the isolated chain acceptance rates for each type of tetrad as a function of the overall P_m of the system. Error bars for *rrr* sequences when $P_m = 0.0$ and *mmm* sequence when $P_m = 1.0$ are shown slightly displaced from the data point. The average error bar for all tetrads over the intermediate range of $P_m = 0.2-0.8$ is shown with the average rate of 0.74 as (0.85, 0.74) on the graph.

intermediate mixed diad environment (overall $P_m = 0.2-0.8$), ~74% of the moves that can occur in isolated chains also can occur in the melt. However, the ratio of melt to isolated chain acceptance rates for *mmm* sequence in iPP and *rrr* tetrads in sPP is much lower than that for their counterparts in the presence of mixed stereochemistries, indicating a greater intermolecular contribution when these tetrads are surrounded by like tetrads. Even at $P_m = 0.2$ when *rrr* tetrads are abundant but not exclusive to the system, there is a noticeable decrease in the melt to isolated chain acceptance ratio for *rrr* tetrads when compared to other tetrads. A similar decrease is seen for *mmm* at $P_m = 0.8$ but cannot be confirmed since the difference is not statistically significant. For the pure stereochemistries, only 25–35% of moves that occur in isolated chains can occur in the melt.

Discussion

From our analysis of the slow-moving beads in each system and the acceptance rates by tetrad, our results suggest that the maximum in the diffusion rate is due to the connectivity of random stereochemical sequences. For stereochemically pure polymers, ones with only *meso* or *racemo* diads, the consistency in the chirality of sequences of monomer units imposes a standard steric hindrance that allows for a dominant chain conformation. In atactic chains, however, the quenched randomness in stereochemical sequences prevents the regularity that allows some configurations to dominate. Recent calculations

have shown that the ability of coarse-grained models to reproduce the dimensions of atactic chains relies more heavily on accurate models of the stereochemical sequences than on the accurate sampling of chain conformations,[3] suggesting the importance of quenched randomness. The low-energy helix or planar zigzag conformations that are predominant in crystalline isotactic or syndiotactic chains, respectively, are present among the random sequences but are not ubiquitous enough to reinforce each other as crystals do. Previous work on PP has conjectured that long-lived, less mobile structures can form in sPP from *all-trans* crystal-like sequences.[13] This was suggested to explain how small fractions of iPP or aPP chains in a sPP melt can lead to demixing. Now have we observed not only these structures and their signatures but also similar structures in iPP. Here the implication is that the addition of small amounts of quenched randomness within the chain may prevent helix and extended chain aggregation, thus enhancing diffusion. Given the difficulty in creating true iPP and sPP samples,[1,2] this result is of interest since high mobility can be enhanced by randomness, rather than relying simply on the high mobility inherent in iPP chains, when compared to sPP.

Because diffusion and the glass transition phenomenon are related through free volume theory, the enhanced diffusion for intermediate stereochemical composition may be indicative of a lowered T_g for atactic chains. Recent work with poly(*tert*-butyl acrylate) has also suggested a U-shaped dependence of T_g on P_m.[28] This effect of random stereochemistry on T_g was not found to be dependent on molecular weight in that case. To confirm our data for diffusion vs P_m at higher molecular weight, we conducted a few representative melt simulations for 100-monomer chains and confirmed the trend, though it is less pronounced. Those simulations are complicated, however, by the onset of entanglements for sPP (but not iPP),[29] making interpretation difficult.

According to the acceptance rate data, the behavior of sequences of pure stereochemical composition are the driving force for the enhanced diffusion at $P_m = 0.75$. The *rrr* and *mmm* tetrads have a different acceptance rate when part of an environment of mixed stereochemical composition than they do when surrounded by like tetrads. When neighboring chains consist of random tetrads, the *mmm* and *rrr* tetrads are more mobile. The fact that acceptance rates for tetrads of mixed stereochemistry do not change significantly based on the overall P_m suggests that quenched randomness plays a larger role in regulating diffusion that the actual value of P_m does.

We can confirm that the decrease of acceptance rates as P_m approaches pure stereochemistry is due to intermolecular effects. At intermediate stereochemical composition, the strong intermolecular packing that causes clustering in pure stereochemistry is blocked by the random nature of the sequences, making crystal-like packing difficult. This is confirmed by the strong decrease in melt/isolated acceptance ratio for the pure stereochemistries, which shows a lower mobility for *mmm* and *rrr* sequences in iPP and sPP, respectively. Therefore, these less mobile structures must be composed of more than one chain segment since the lack of mobility cannot be explained by RIS intramolecular interactions alone.

The characteristics of these slow-moving clusters of beads are further elucidated by the intra- and intermolecular distance correlations between unmoved beads over a time interval. The intermolecular pair distribution function reveals that unmoved beads cluster in all systems but that the size of these clusters is larger for stereochemically pure melts. The populations of the distances between unmoved beads within the same molecule

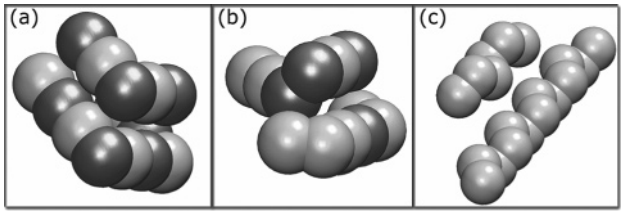

Figure 9. Representative snapshots of clusters of the slowest-moving beads in sPP (a), aPP (b), and iPP (c). Dark gray beads represent an *l*-configuration stereochemistry, and light gray are *d*-configurations (images rendered using Visual Molecular Dynamics,[27] version 1.8.3).

reveal that the dominant crystal-like conformations are most prevalent in the clusters. For the case of aPP, where no dominant conformation exists, the clusters are stochastic in conformation and are short-lived. Figure 9 shows some representative samples of these structures from the analysis of temporarily immobile beads, discussed in the previous section. For iPP, the snapshot shows two neighboring segments in the $tg^{\pm}$ helix conformations. The prevalence of increased populations of intramolecular correlations for up to 10 Å along the chain (in Figure 7) suggests that up to eight torsion angles may be participating in the helices, taking on variations the conformation $g^{\pm}tg^{\pm}tg^{\pm}tg^{\pm}t$. The intermolecular distances between close beads in two neighboring helices can range from 6 to 9 Å, corresponding to the first intermolecular peak of iPP in Figure 6. The subsequent peaks suggest that a few clusters make contain more than three helices, generating longer range intermolecular correlations. For sPP, combinations of both the most common *tt* conformation and also probable $g^{\pm}g^{\pm}$ conformation are seen in this representative cluster in Figure 9, confirmed by the sPP peaks in Figure 7. For zigzag planar conformations, an intermolecular spacing of 5−8 Å is expected and seen in Figure 6. The atactic case of $P_m = 0.6$ in Figure 9 generates a cluster with no dominant conformation. The length scale of the cluster, which is seen in Figure 6, is also much smaller than that of iPP or sPP. Because the time interval required to find a comparable percentage of unmoved beads is so small compared to that of iPP and sPP, the aPP clusters can be described as small structures that do not last long, with no signature conformations, suggesting that the clustering that we find in atactic chains is not of the same nature of those long-lived clusters in stereochemically pure melts that lead to the decrease in mobility. The clustering in aPP is similar to the spatially heterogeneous dynamics recently studied in glass-forming liquids.[30] Dominant conformations in crystal-forming iPP and sPP create a higher level of heterogeneity, which variations in stereochemistry can counter.

Conclusions

The melt diffusion of isotactic, atactic, and syndiotactic polypropylene (PP) is studied over the entire range of stereochemical composition by dynamical Monte Carlo. The technique uses realistic two-bead moves to obtain diffusion coefficients for a stereochemistry-dependent, coarse-grained model of polypropylene derived from the rotational isomeric state (RIS) model and repulsive Lennard-Jones interactions. Increased diffusion of isotactic PP, compared to syndiotactic PP, is reproduced. Faster diffusion at intermediate stereochemical composition is also found. We study distributions of displacements over time to determine the origin of the fast diffusion, focusing on the fractions of unmoved beads. We compare pair correlation functions of the unmoved beads to those of all beads to determine the characteristics of these slow-moving beads. We find the clusters of slow-moving beads in iPP and sPP are long-lived and resemble the crystalline form of the material,

while clusters in aPP appear to be short-lived with no dominant conformations. Randomness of the stereochemical sequence works against the occasional formation of relatively long-lived immobile clusters in aPP melts, as compared to the situation in the stereochemically pure iPP and sPP melts. Monte Carlo acceptance rates, characterized by the stereochemistry of the local tetrad and overall stereochemical composition, reveal that sequences of pure stereochemistry diffuse faster in melts with quenched randomness of stereochemical sequences than in stereochemically pure melts, while sequences of random stereochemistry are relatively unaffected. Comparison to isolated chain acceptance rates indicates that intermolecular cohesiveness of stereochemically pure sequences is responsible for the crystal-like structures that lower mobility, which can be broken up by the quenched randomness of atactic sequences.

Acknowledgment. This research was supported by National Science Foundation Grant DMR0455117.

References and Notes

(1) Eckstein, A.; Suhm, J.; Friedrich, C.; Maier, R. D.; Sassmannshausen, J.; Bochmann, M.; Mulhaupt, R. *Macromolecules* **1998**, *31*, 1335−40.
(2) Lippow, S. M.; Qiu, X. H.; Ediger, M. D. *J. Chem. Phys.* **2001**, *115*, 4961−5.
(3) Mattice, W. L.; Waheed, N. *Macromolecules* **2006**, *39*, 2380−7.
(4) Edwards, S. F.; Vilgis, T. A. *Rep. Prog. Phys.* **1988**, *51*, 243−97.
(5) Soteros, C. E.; Whittington, S. G. *J. Phys. A: Math. Gen.* **2004**, *37*, R279−R325.
(6) Flory, P. J. *Statistical Mechanics of Chain Molecules*; Wiley: New York, 1969.
(7) Ahumada, O.; Theodorou, D. N.; Triolo, A.; Arrighi, V.; Karatasos, C.; Ryckaert, J. P. *Macromolecules* **2002**, *35*, 7110−24.
(8) Arrighi, V.; Batt-Coutrot, D.; Zhang, C. H.; Telling, M. T. F.; Triolo, A. *J. Chem. Phys.* **2003**, *119*, 1271−8.
(9) Antoniadis, S. J.; Samara, C. T.; Theodorou, D. N. *Macromolecules* **1999**, *32*, 8635−44.
(10) Destree, M.; Laupretre, F.; Lyulin, A.; Ryckaert, J. P. *J. Chem. Phys.* **2000**, *112*, 9632−44.
(11) Haliloglu, T.; Mattice, W. L. *J. Chem. Phys.* **1998**, *108*, 6989−95.
(12) Haliloglu, T.; Mattice, W. L. *J. Chem. Phys.* **1999**, *111*, 4327−33.
(13) Clancy, T. C.; Putz, M.; Weinhold, J. D.; Curro, J. G.; Mattice, W. L. *Macromolecules* **2000**, *33*, 9452−63.
(14) Clancy, T. C.; Mattice, W. L. *J. Chem. Phys.* **2001**, *115*, 8221−5.
(15) Xu, G. Q.; Clancy, T. C.; Mattice, W. L.; Kumar, S. K. *Macromolecules* **2002**, *35*, 3309−11.
(16) Mattice, W. L.; Helfer, C. A.; Rane, S. S.; von Meerwall, E. D.; Farmer, B. L. *J. Polym. Sci., Part B: Polym. Phys.* **2005**, *43*, 1271−82.
(17) Lin, H.; Mattice, W. L.; von Meerwall, E. D. *J. Polym. Sci., Part B: Polym. Phys.* **2006**, *44*, 2566−71.
(18) Rapold, R. F.; Mattice, W. L. *J. Chem. Soc., Faraday Trans.* **1995**, *91*, 2435−41.
(19) Orwoll, R. A. In *Physical Properties of Polymers Handbook*; Mark, J. E., Ed.; American Institute of Physics: Woodbury, NY, 1996; p 81.
(20) Suter, U. W.; Pucci, S.; Pino, P. *J. Am. Chem. Soc.* **1975**, *97*, 1018−23.
(21) Mattice, W. L.; Suter, U. W. *Conformational Properties of Large Molecules. The Rotational Isomeric State Model in Macromolecular Systems*; Wiley: New York, 1994.
(22) Doruker, P.; Mattice, W. L. *Macromolecules* **1997**, *30*, 5520−6.
(23) Cho, J. H.; Mattice, W. L. *Macromolecules* **1997**, *30*, 637−44.
(24) Clancy, T. C.; Mattice, W. L. *J. Chem. Phys.* **2000**, *112*, 10049−55.
(25) Allen, M. P.; Tildesley, D. J. *Computer Simulations of Liquids*; Oxford University Press: New York, 1987.
(26) Williams, G.; Watts, D. C. *Trans. Faraday Soc.* **1970**, *66*, 80.
(27) Humphrey, W.; Dalke, A.; Schulten, K. *J. Mol. Graphics* **1996**, *14*, 33.
(28) Liu, W. H.; Nakano, T.; Okamoto, Y. *Polymer* **2000**, *41*, 4467−72.
(29) Fetters, L. J.; Lee, J. H.; Mathers, R. T.; Hustad, P. D.; Coates, G. W.; Archer, L. A.; Rucker, S. P.; Lohse, D. J. *Macromolecules* **2005**, *38*, 10061−6.
(30) Lacevic, N.; Starr, F. W.; Schroder, T. B.; Glotzer, S. C. *J. Chem. Phys.* **2003**, *119*, 7372−87.

MA062285R